COMPUTER-FOCUSING FOR AREA SCANS

T. Nagai, T. A. Iinuma and S. Koda

National Institute of Radiological Sciences, Chiba, Japan

Scintillation area scanning is a relatively new diagnostic method in clinical medicine and its use has progressed rapidly over the years. Because the method is used to visualize the spatial distribution of radioactivity in internal organs, one would like to be able to detect and display the smallest possible lesions. Many methods using a wide range of instruments and radiopharmaceuticals have been advocated to increase the resolving power of the scanner.

At the present time, however, the resolution of area scanners is not sufficiently sharp. A multichannel focusing collimator consisting of a honeycomb of hexagonal holes is usually used, but even with this focusing collimator the region of response is broad and has a circular cross section at the focal distance. The sensitivity in scanning must also be increased, but at present this can be achieved only by sacrificing spatial resolution.

In a previous paper (*1*) we reported that a correction method based on iterative approximation which had been used to correct distortion in beta and gamma spectra (*2*) could be used to extract true information from the observed data; with this method corrected profiles obtained with a whole-body linear scanner showed a more detailed structure than did the original. We felt that a similar correction method could be used in the image of area scans.

At present a wide variety of analog techniques are used to record area-scanning data. These analog techniques, however, appear to offer less accurate recording and result in a loss of information. Moreover, they are not adaptable to computer analysis. To use digital-computer processing, it is necessary to use digital recording in which all original information in an unmodified form is collected and recorded as an array of actual numbers.

The purpose of this paper is to show how digital information suitable for computer processing can be used and how more information can be obtained from computer-corrected area scans than from the original digital scan or conventional analog data presentation.

METHODS

The data-collection system consisted of a commercial scanner with a NaI(Tl) crystal, 2 in. in diameter and 2 in. thick, and a 19-hexagonal-hole honeycomb collimator. Pulses from a single-channel pulse-height analyser were fed into a 128-channel multichannel analyser used in the multiscaling mode. Because a bidimensional multiscaler was not available, the single-dimensional 128-channel multiscaler was used to present a numerical profile for each scan sweep.

One-way scanning was done at a speed of 2.7 mm/sec, and 1-mm spacing was selected. The preset counting time in each channel of the multiscaler was 0.38 sec. Consequently each channel corresponded to the accumulation of counts from a length of 1 mm of scan sweep at the scanning speed selected. The recording of the counts for each sweep was started just when the reference point of the detector passed over the scan registration line which met the scan sweep direction at right angles in order to include precise positional information. After each scan sweep, the counts accumulated in each of the 128 channels were printed with a Hewlett Packard fast printer. During the printing the detector returned to the next starting point but spaced 1 mm perpendicular to the sweep direction. Then the multiscaler started to accumulate counts for the next scan sweep.

A channel number corresponded to the position of the detector in each scan sweep, and the number of the sweep corresponded to the position in the space direction. Thus to provide a two-dimensional array of numbers representing area scanning data,

Received Nov. 17, 1966; revision accepted Aug. 24, 1967.

For reprints contact T. Nagai, IAEA, Section of Nuclear Medicine, Kaerntnerring 11, Vienna, Austria.

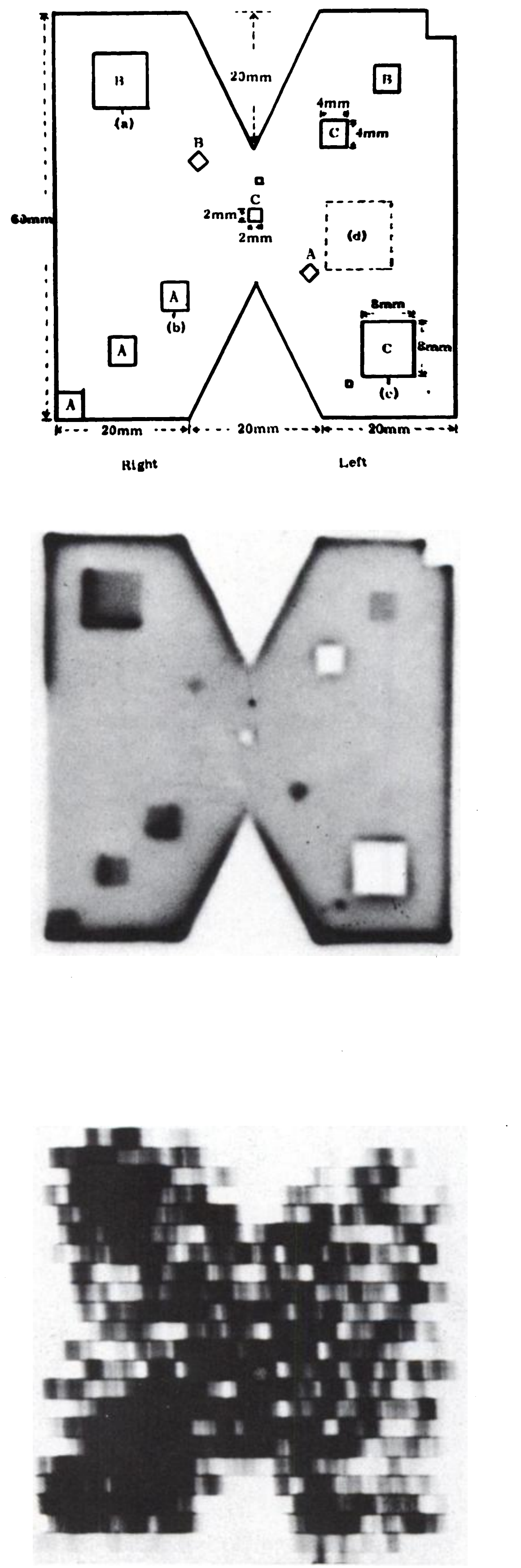

FIG. 1. Diagram, autoradiogram and conventional photoscan of thyroid phantom containing hot and cold mock tumors.

the sweep was repeated to cover the entire scanned area.

Optimal size of the unit area may depend upon the resolution of the collimator, and in the present study the unit area to which each count in the array corresponded was chosen to be 1 mm^2.

A simple paper phantom simulating a thyroid gland was constructed to evaluate the efficiency of our method. So that the number of counts in the unit area would be as statistically meaningful as possible, the phantom contained a rather large amount of ^{131}I—650 μc. Thirteen hot and cold mock tumors of various sizes were placed on the phantom. A diagram of the phantom is shown in Fig. 1 together with its autoradiogram and conventional photoscan. Items A are tumors loaded with three times the radioactivity, and items B have two times the radioactivity of the remaining area. Items C are cold tumors with no radioactivity. An unexpectedly high concentration of radioactivity on the perimeter was caused by a capillary phenomenon and is seen on the phantom as shown in the autoradiogram.

The phantom was placed at a focal distance of 6 cm, and the scanning was performed in air. The counts at 360 $\pm$ 50 kev varied from 14 to 1,336 counts, and background counts were between 0 and 3 per unit area. The array of counts obtained consisted of 126 $\times$ 87 elements.

Because scan data of a point source that were a fundamental measure of the resolution characteristics of the collimator were needed for a "computer-focusing" method, a ^{131}I point source with a 2-mm diameter was scanned in exactly the same way. From the data obtained, a 21 $\times$ 21 = 441 element array of counts was selected for computer processing.

COMPUTER PROCESSING

In processing the digital scan obtained the computer program undertook the following steps: 1. background subtraction, 2. smoothing the original data, 3. iterative approximation to approach true distribution and 4. again smoothing the corrected data. The recorded array of counts was punched onto computer cards and then fed into a Burroughs-5500 digital computer. The computer time for this procedure was approximately 28 min.

Although background subtraction can be preset at any level, in this case background counts in each unit area were so small that the subtraction was not performed.

Because the accumulated counts have inherent statistical variation, a data-smoothing technique is necessary, especially when the counting rate is low. This smoothing can be performed by a computer.

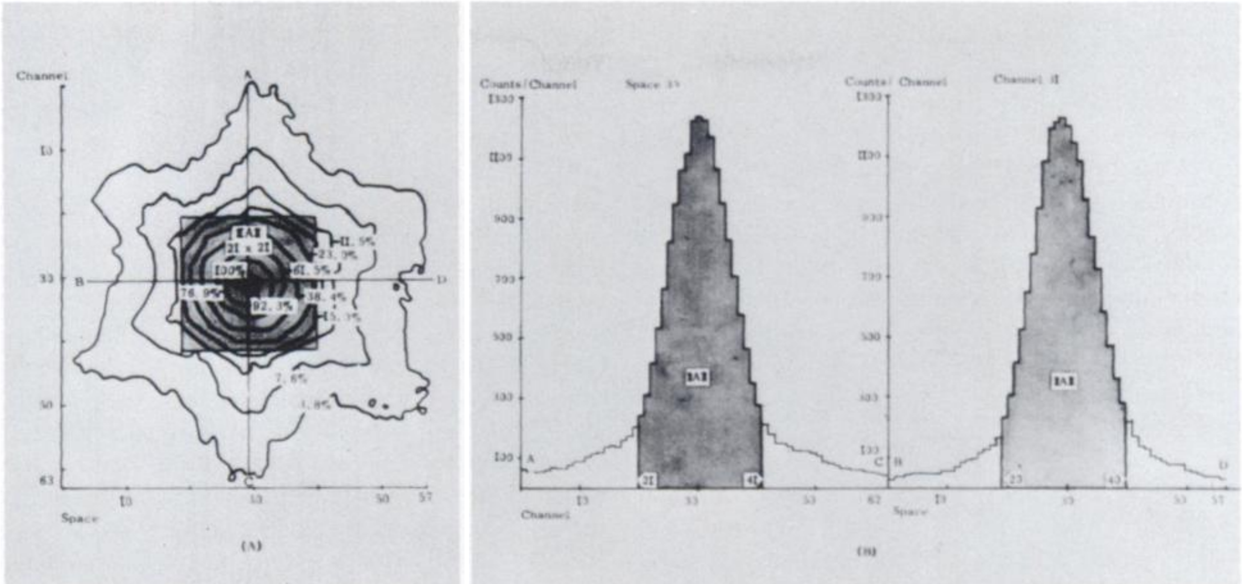

FIG. 2. Digital-to-analog converted isocount contour map of point source shows that point source appears many times larger and is shaped like six-armed starfish—the exact shape depending on collimator used. B gives transverse response profiles obtained from lines marked on A. Shaded area represents resolving power array $||A||$.

Each number was compared to the mean of its surrounding eight neighbors to determine whether or not it was significantly different. If it was more than one standard deviation away from the mean, it was replaced by the mean. In this way, smoothing was performed for the data of the point source and the thyroid phantom. After this initial smoothing, further computer processing was done to correct the "blur" due to lack of resolution of the collimator. Since the correction procedure has been described in a previous paper (*1*), only a brief explanation is given here.

For convenience, the following notations are defined;

- $||X||$ original scanning data after smoothing, expressed in a two-dimensional array form (original image).
- X_{ij} an element in array $||X||$ that corresponds to a counting rate per unit area (the ith column of the jth row); total number of elements are nm (original elements).
- $||A||$ resolving power array of a collimator that is obtained by scanning a point source of unit activity.
- A_{oo} a central element of $||A||$ that corresponds to a counting rate when a collimator is coaxially placed with a point source.
- A_{kl} an element of $||A||$ that corresponds to a counting rate when the collimator is displaced a certain distance from the point source. ΣA_{kl} is normalized to unity.

The iterative approximation proceeds as follows; for simplicity calculation of an element X_{ij} is shown.

In the first approximation

$$X^1_{ij} = X_{ij} + (X_{ij} - \sum_{kl} A_{kl} X_{i+k, j+l}) \qquad (1)$$

where $\Sigma A_{kl} X_{i+k, j+l}$ means that the multiplication starts from $A_{oo} X_{ij}$; then A_{kl}, which corresponds to a certain distance from A_{oo}, should be multiplied by $X_{i+k, j+l}$, which corresponds to an identical distance from X_{ij}. The same process is repeated for all A_{kl}. The calculation of Eq. 1 must be performed for all X_{ij}.

Similarly the ith approximation is

$$X^i_{ij} = X^{i-1}_{ij} + (X_{ij} - \Sigma A_{kl} X^{i-1}_{i+k, j+l}) \qquad (2)$$

The approximation was stopped when $\Sigma A_{kl} X^i_{ij}$ agreed with X_{ij} within the statistical standard deviation $(X_{ij})^{1/2}$. For all nm unit areas, the limit of approximation is (see Appendix)

$$\sum_{nm} \frac{(X_{ij} - \Sigma A_{kl} X^i_{i+k, j+l})^2}{X_{ij}} \leq nm. \qquad (3)$$

In the present case $||X||$ was obtained as a 126 $\times$ 87 array which corresponded to a far larger area than that of the original phantom. For $||A||$ the number of elements was restricted to 21 $\times$ 21 = 441. The elements outside this array have negligible values compared to those inside, as shown in Fig. 2.

Consequently, the iterative calculation could be performed for the X_{ij} which satisfied the conditions $11 \leq i \leq 116$ and $11 \leq j \leq 77$. Thus the number of corrected elements was 106 $\times$ 67 = 7,102, corresponding to the nm in Eq. 3.

After an iteration was completed, Eq. 3 was calculated automatically by the computer, and the calculated value was compared to 7,102. For the present case, the values were 10,870, 7,436 and 5,998 for first, second and third iterations, respectively, and convergence of the value was quite satisfactory. According to the criterion of Eq. 3, the iteration was stopped at the third time. To prevent oscillations in the solution of the iterative approximation, smoothing was again necessary for X^1_{ij}, X^2_{ij} and X^3_{ij}, respectively. These final results were compared with the original elements X_{ij} and the autoradiogram of the phantom.

RESULTS

Because the immediate visual impression may be lost with fully digital display because the patterns are presented as an array of complicated numbers, some interpolation is necessary such as drawing color scans or isocount contour lines. In this case color scans and isocount contours were plotted manually from the digital display obtained to help the human visual system in the interpretation.

Figure 2 A shows a digital-to-analog converted isocount contour map of the point source. It shows that a point source appears many times larger and is shaped like a six-armed starfish, the exact shape depending on the focusing collimator used.

Figure 2 B gives the transverse response profiles obtained from the lines marked on Fig. 2 A. The shaded areas represent the resolving power array $||A||$. A portion of the resolving power array normalized to unity is shown in Table 1.

Digital-to-analog converted isocontour maps of the thyroid phantom are shown in Fig. 3. Note that the difference in apparent amount of radioactivity is much greater in the computer-corrected scan (B) than in the smoothed original scan (A).

Figures 3 C, D and E show profiles obtained at the lines marked on Figs. 3 A and B. Peaks and troughs barely distinguishable on the smoothed original profiles are obvious on the corrected profiles, and the corrected curves show more of the detailed structure of the distribution. The minimum in the profile (D) represents the interlobular space, and the curve clearly shows a depression from the cold tumor in the lower pole of the left lobe.

The effect of continued iterations on profile curves obtained at the line marked a — b on Figs. 3 A and B can be seen in Fig. 4, which shows the first, second and third iterative approximations. This is evidence that the approximations converge satisfactorily. and the figure shows that our procedure yields a good approximation after a few iterations in this case.

Table 2 shows one of the features of the smoothed original array of the actual counts accumulated per unit area as compared to the features of the computer-corrected pattern shown in Table 3. Both

TABLE 1. PARTIAL FEATURES OF A ARRAY NORMALIZED TO UNITY

	Space No.						
Channel No.	28	29	30	31	32	33	34
21	0.001018	0.001077	0.001044	0.001074	0.001041	0.000998	0.001005
22	0.001371	0.001388	0.001468	0.001421	0.001397	0.001367	0.001282
23	0.001812	0.001987	0.001923	0.001824	0.001764	0.001722	0.001421
24	0.002362	0.002419	0.002452	0.002412	0.002290	0.002131	0.001820
25	0.002919	0.002985	0.003031	0.002897	0.002839	0.002586	0.002182
26	0.003621	0.003691	0.003636	0.003639	0.003519	0.003069	0.002669
27	0.004034	0.004233	0.004340	0.004271	0.004155	0.003715	0.003252
28	0.004466	0.004777	0.005060	0.004924	0.004679	0.004202	0.003766
29	0.004777	0.005217	0.005571	0.005338	0.005052	0.004703	0.004280
30	0.005193	0.005483	0.005668	0.005538	0.005230	0.004792	0.004452
31	0.005263	0.005673	0.005743*	0.005659	0.005431	0.004925	0.004412
32	0.005145	0.005477	0.005617	0.005629	0.005357	0.004906	0.004415
33	0.004856	0.005187	0.005357	0.005397	0.005132	0.004764	0.004271
34	0.004549	0.004792	0.005079	0.004904	0.004758	0.004405	0.003874
35	0.004173	0.004326	0.004484	0.004531	0.004220	0.003900	0.003389
36	0.003630	0.000808	0.003844	0.003901	0.003846	0.003666	0.003329
37	0.002938	0.003171	0.003261	0.003398	0.003305	0.003129	0.002771
38	0.002351	0.002590	0.002660	0.002739	0.002637	0.002428	0.002293
39	0.001857	0.002066	0.002103	0.002196	0.002098	0.002001	0.001913
40	0.001463	0.001591	0.001665	0.001712	0.001671	0.001569	0.001483
41	0.001161	0.001253	0.001295	0.001336	0.001311	0.001219	0.001100

* Corresponds to a central element A_{oo}.

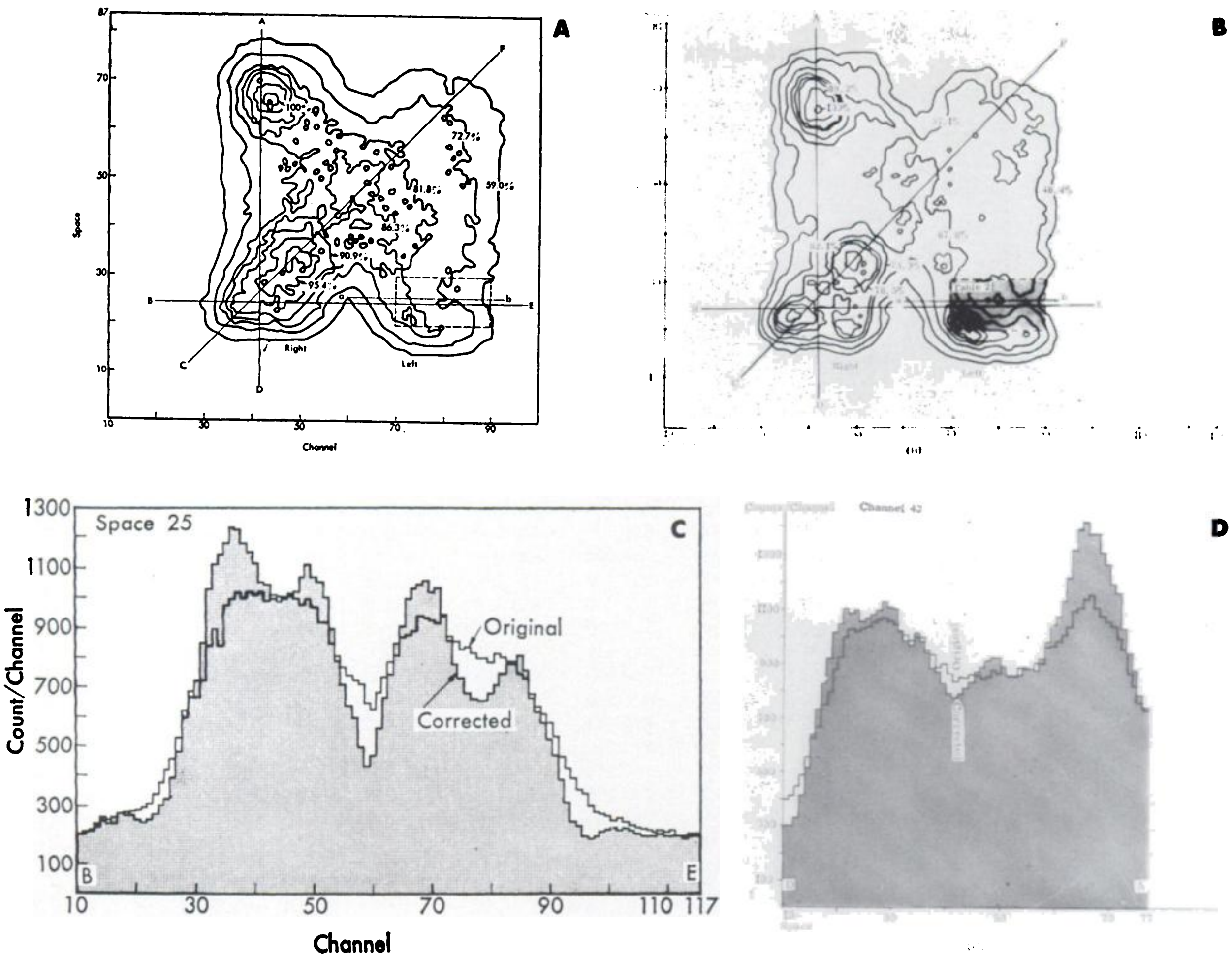

FIG. 3. Digital-to-analog converted isocontour maps of thyroid phantom. Difference in apparent amount of radioactivity is much greater in computer-corrected scan (B) than in smoothed original scan (A). C, D (above) and E (below) show profiles obtained at lines marked in A and B. Peaks and troughs barely distinguishable on smoothed original profiles are obvious on corrected profiles.

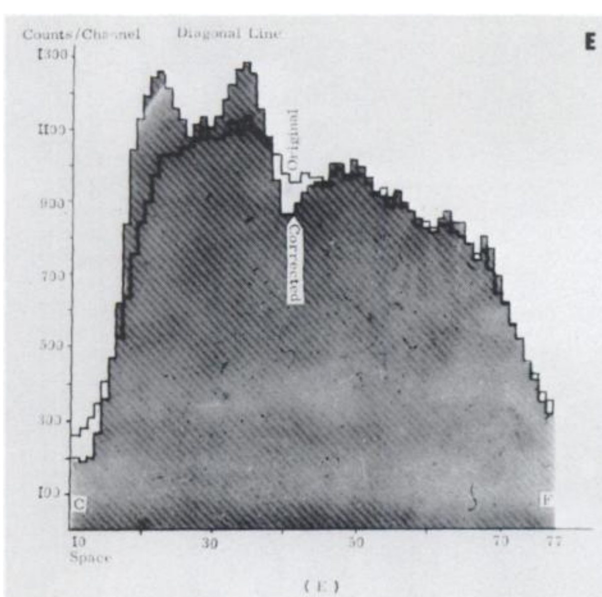

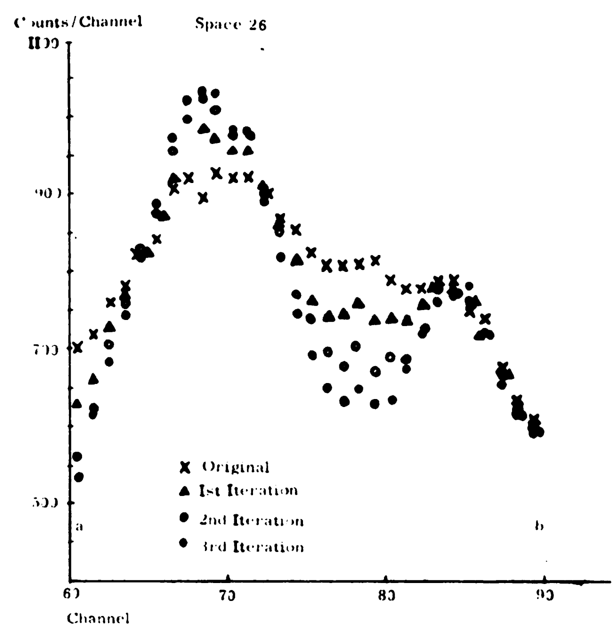

FIG. 4. First, second and third iterative approximations on profile curves obtained at line marked (a–b) in Fig. 3A and B.

tables correspond to the shadow area on Fig. 3 A and B.

In Fig. 5 digital-to-analog converted color displays of the phantom are shown, together with charts showing the relation between counts per unit area and colors. The colors are chosen arbitrarily, each color corresponding to a given number of counts, and each element corresponding to an area of 1 mm².

TABLE 2. ONE OF FEATURES OF COMPUTER-SMOOTHED ARRAY OF THYROID PHANTOM*

Channel No.	Space No. 21	22	23	24	25	26	27	28	29	30
70	882.671	904.438	929.000	922.323	933.165	926.271	932.000	917.875	903.000	942.000
71	896.000	925.389	933.000	945.000	925.000	921.555	909.000	903.984	905.607	902.201
72	938.000	950.000	970.000	944.000	918.000	924.944	905.810	906.800	887.000	898.851
73	929.951	934.000	971.000	950.000	944.000	902.844	888.000	905.000	881.206	874.000
74	952.000	952.000	915.000	920.000	871.000	867.000	873.856	866.000	871.026	885.000
75	946.000	925.000	918.000	898.000	858.000	854.000	869.000	839.000	849.000	869.000
76	934.000	936.000	901.000	861.000	834.000	825.000	830.000	842.000	853.000	867.000
77	895.000	888.000	885.750	862.000	837.250	810.000	822.125	808.000	808.000	833.000
78	864.000	866.219	855.000	842.000	815.000	808.297	787.000	826.000	821.500	838.188
79	873.000	861.277	862.000	816.000	798.000	810.287	806.198	792.000	808.211	833.000
80	870.000	856.910	810.000	798.000	797.661	813.000	788.061	775.000	795.000	785.000
81	874.000	828.364	836.000	802.000	786.000	787.965	765.000	785.000	804.000	802.000
82	818.000	830.170	818.192	814.000	811.000	778.000	765.000	790.000	777.000	784.000
83	850.000	812.000	845.000	809.399	800.425	779.803	776.000	802.000	785.125	771.000
84	835.968	852.000	840.000	808.000	782.000	785.000	781.350	799.000	779.000	779.000
85	818.000	825.621	819.328	792.541	780.943	788.000	774.169	776.000	784.000	798.000
86	803.000	804.994	823.000	799.000	743.000	750.000	756.000	758.000	770.000	769.578
87	783.896	794.000	777.374	767.000	736.000	743.000	726.875	738.359	762.000	741.185
88	764.612	750.485	744.482	734.000	676.000	676.000	683.000	700.154	706.000	697.398
89	707.000	698.697	719.000	657.000	635.000	632.000	644.269	633.000	644.000	669.002
90	662.962	681.000	643.000	626.000	609.000	609.784	630.000	638.000	621.000	654.000

* Numbers represent the actual counts accumulated per unit area.

TABLE 3. ONE OF FEATURES OF THE COMPUTER-CORRECTED ARRAY OF THYROID PHANTOM*

Channel No.	Space No. 21	22	23	24	25	26	27	28	29	30
70	1129.557	1131.940	1112.050	1083.315	1052.715	1034.237	988.587	975.363	975.341	957.814
71	1125.139	1162.182	1129.329	1087.302	1019.217	987.432	963.503	907.982	912.491	897.093
72	1148.363	1164.477	1134.283	1095.165	1028.629	986.300	909.599	918.525	887.591	893.720
73	1176.238	1120.100	1091.584	1015.536	939.003	893.592	841.262	848.484	835.394	853.377
74	1161.186	1094.895	1026.518	928.387	856.578	820.003	796.435	782.432	816.633	826.096
75	1147.007	1052.280	983.673	852.338	772.280	745.640	732.704	760.075	804.457	846.137
76	1077.914	992.559	918.962	809.129	728.021	695.294	693.211	735.964	757.516	798.177
77	986.037	906.969	837.221	763.729	674.019	653.179	660.342	690.369	754.978	815.586
78	950.856	879.005	798.088	706.623	658.696	636.343	665.707	691.190	738.811	819.341
79	960.441	838.282	742.616	666.073	652.592	652.007	663.870	676.482	720.923	757.649
80	942.239	849.656	736.113	679.680	653.973	632.167	626.616	676.894	702.682	772.279
81	905.361	823.301	782.239	710.433	678.375	635.756	654.454	678.569	723.799	777.655
82	912.755	856.506	796.827	766.318	703.842	677.843	700.456	737.209	749.543	741.609
83	938.790	917.247	858.391	794.578	746.747	724.350	758.951	770.865	778.260	781.518
84	976.031	935.479	877.742	814.879	784.758	763.427	774.266	799.499	802.449	842.438
85	965.363	963.479	922.159	850.593	783.075	769.934	803.489	829.861	877.850	866.538
86	976.481	951.998	919.900	837.555	801.274	783.233	797.682	822.722	884.844	888.733
87	979.315	936.573	906.068	813.206	753.150	722.453	756.501	817.986	817.657	846.499
88	924.866	904.467	831.135	739.209	667.092	655.897	665.850	704.902	732.389	751.123
89	855.409	830.897	750.068	664.519	619.300	619.597	639.315	667.261	708.346	726.671
90	781.009	742.165	661.828	593.720	577.972	595.640	613.773	629.995	665.965	674.811

* Area corresponds to that shown in Table 2.

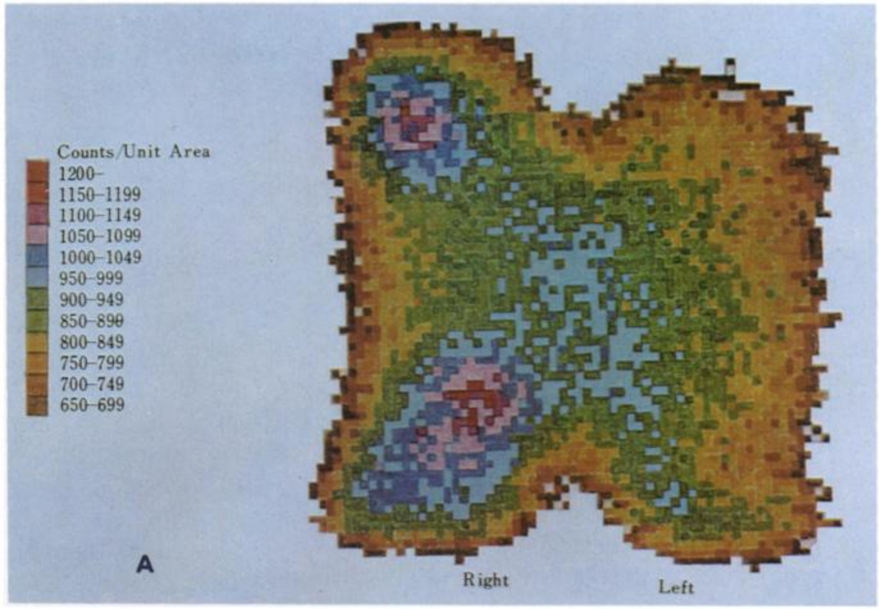

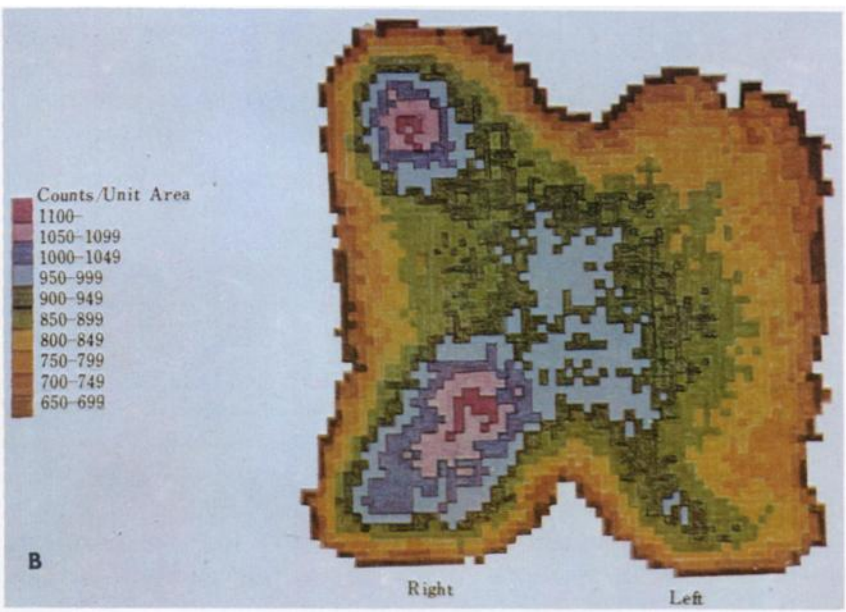

FIG. 5. Digital-to-analog converted color displays of phantom are shown together with charts with relation between counts per unit area and colors. Each color corresponds to given number of counts and each element corresponds to area of 1 mm^2. A shows original scan, B shows smoothed scan and C shows digital-to-analog converted color scan resulting from iterative approximation.

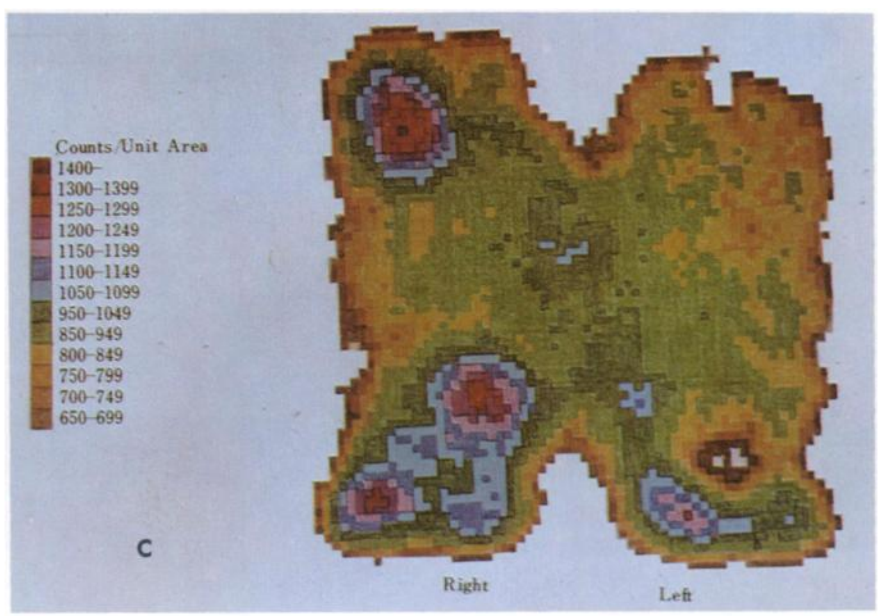

It can be said that significantly better diagnostic information is available from the original scan (A) than the conventional photoscan. Visual impression is remarkably improved on the smoothed original scan (B), but the detailed structures are still not good enough.

Figure 5 C shows the digital-to-analog converted color scan resulting from iterative approximation. The corrected scan shows tumors strikingly clearly which can only be suspected or cannot be seen on the smoothed original scan. The three hot tumors in the right lobe are clearly separated. Note the marked increase in contrast of the cold tumor in the lower pole of the left lobe. The variations in intensity that are not observed over two small hot tumors in the central area and over the edge areas of the phantom on the smoothed original scan are obvious on the corrected scan. A small defect (e) due to an artifact is observed.

The contrast ratios, normalized to the isotope concentration of a central area (d) marked in Fig. 1, are shown in Table 4. The ratios are compared to actual values obtained by a well-type scintillation counter. This suggests that the ratios observed in the corrected data are much closer to the actual ratios than those obtained from the smoothed original data, but it seems too early to draw conclusions from this preliminary quantitative estimation.

DISCUSSION

Generally, methods for recording scan data rely on analog means, and much of the difficulty in interpreting scans results from subjective methods. Recently, however, the availability of fast automatic digital-recording devices makes it possible to obtain numerical display of scans. Thus today, to prevent the loss of data and the introduction of a time lag by analog instruments such as a counting-rate meter, conventional scanners are being replaced in some instances by actual digital scanners. Digital display provides exact data, but the vast quantities of numerical data in area scanning virtually requires the use of a digital computer.

Although the current literature (*3–22*) describes a number of computer techniques for scan interpretation, not enough attention has been paid to the correction for finite resolution of the collimator. Computer techniques open up the possibility of correction of this complex problem.

We have developed a new computer-processing method, "computer-focusing," to reduce the "blur" in display due to lack of resolution of the focusing collimator and to provide increased accuracy in area scanning. In the preliminary study this method provided a satisfactorily focused display without the serious noise that is usually encountered in the Fourier transform method. Moreover, the calculation was quite simple, and the programming procedure for the computer was not very complex although time required for the computation was large.

In routine clinical applications, computation may be stopped after one or two iterative approximations because of the rapid convergence of Eq. 3. Thus the optimal compromise might be found between the resulting focused images and the cost of running the computer for each particular application. It has also been shown that the focused image may indicate not only the exact size of lesions or organs, but also the total amount of radioactivity in organs and the percent of total activity in any lesion. In the case of area scanning, however, this method is valid only under the assumption that the resolution is not affected much by the depth of the source in tissue.

In the present case, digital-to-analog converted color displays and isocount contours were drawn manually from the numerical data. Automated recording using isocontour lines or characters of increasing density, however, may possibly be accomplished by computer processing in the near future.

In principle, this computer-focusing technique can be applied to any type of scanning. one, two and three-dimensional images obtained by either moving or stationary devices. provided the data are available in digital form. However, the amount of calculation would increase enormously in the case of three-dimensional focusing.

Because the resolution depends on the collimator and the gamma-ray energy, one should make a catalog of the resolving power of a certain collimator

TABLE 4. QUANTITATIVE MEASUREMENTS OF RADIOACTIVITY IN TUMORS

	Observed contrast ratios		
	Well-type scintillation counting	Smoothed data	Corrected data
Hot tumor (a)	3.252	1.884	2.956
Hot tumor (b)	5.116	2.176	3.029
Cold tumor (c)	0.000	0.504	0.001
Reference area (d)	1.000	1.000	1.000

for various radionuclides, and then the focusing can be made for an observed scan image according to the radionuclide used.

High-resolution scans with high-energy gamma emitters, such as ^{132}I ^{86}Rb, ^{60}Co and ^{47}Ca, etc., which have been difficult to obtain by conventional methods might be attainable with this correction technique. Moreover, the method may be used to analyze radioisotope images with smaller amounts of tracers because digital recording has a markedly greater sensitivity. Although our method requires more time at present, it may be expected that digital imaging device and on-line computer systems can be used to visualize immediately a multidimensional pattern and to perform the "computer-focusing" in a very short time.

SUMMARY

A method for iterative approximation with a digital computer to approach the true isotope distribution in area scanning has been developed. This "computer-focusing" technique offers a means of decreasing the "blur" in area-scan images introduced by lack of resolution of the collimator, providing more accurate information.

ACKNOWLEDGMENT

The authors are indebted to the Japan Information Processing Service Co. for assistance in computer programming. The program for this correction is available in an Algol format. Details should be requested from T. Nagai.

REFERENCES

1. Iinuma, T. A. and Nagai, T.: Repetitive correction for a finite resolving power of the collimator in scintiscanning. *Intern. J. Appl. Radiation Isotopes.* To be published.

2. Skarsgard, L. D., Johns, H. E. and Green, L. E. S.: Iterative response correction for a scintillation spectrometer. *Radiation Res.* **14**:261, 1961.

3. Brown, D. W.: Digital computer analysis and display of the radioisotope scan. *J. Nucl. Med.* **5**:802, 1964.

4. Beattie, J. W. and Bradt, G.: Digital printout system for whole body scanner. *IRE Inst. Radio Engrs. Trans. Bio-Med. Electron.* **8**:24, 1961.

5. Harris, C. C., Bell, P. R., Francis, J. E., Jordan, J. C. and Satterfield, M. M.: Data recording for radioisotope scanning. In *Progress in Medical Radioisotope Scanning.* US-AEC, 1962, p. 66.

6. Kenny, P. J., Laughlin, J. S., Weber, D. A., Corey, K. R. and Greenberg, E.: High-energy gamma-ray scanner. In *Medical Radioistope Scanning,* Vol. 1, IAEA, Vienna, 1964, p. 253.

7. Corey, K. R., Kenny, P. J., Greenberg, E. and Laughlin, J. S.: Detection of bone metastases in scanning studies with calcium-47 and strontium-85. *J. Nucl. Med.* **3**:454, 1962.

8. Laughlin, J. S., Kenny, P. J., Corey, K. R., Greenberg, E. and Weber, D. A.: Localization and total body high-energy gamma-ray scanning in cancer patients. In *Medical Radioisotope Scanning,* Vol. 1, IAEA, Vienna, 1964, p. 253.

9. Tubiana, M.: Discussion. In *Medical Radioisotope Scanning,* Vol. 1, IAEA, Vienna, 1964, p. 497.

10. Kawin, B. and Huston, F. V.: Digital or analog methods for radioisotope measurement?, *Nucleonics* **22**: No. 7, 86, 1964.

11. Mallard, J. R. and Inst, F.: Medical radioisotope scanning. *Phys. Med. Biol.* **10**:309, 1965.

12. Myers, M. J., Kenny, P. J. and Laughlin, J. S.: Quantitative analysis of data from scintillation cameras. *Nucleonics* **24**: No. 2, 58, 1966.

13. Pricher, F. J., Horn, E. G., Reeves, R. J. and Buffalo, T.: Design and properties of the whole body scanner at Duke. *J. Nucl. Med.* **6**:389, 1965.

14. Kawin, B. and Huston, F. V.: Dataphone computer system for radioisotope scan display. *Proc. 16th Ann. Conf. Engl. Med. Biol.* **5**:120, 1963.

15. Aronow, S.: Computer techniques. *Nucleonics* **21**: No. 10, 66, 1963.

16. Kawin, B., Huston, F. V. and Cope, C. B.: Digital processing display system for radioisotope scanning. *J. Nucl. Med.* **5**:500, 1964.

17. Schepers, H. and Winkler, C.: An automatic scanning system, using a tape perforator and computer techniques. In *Medical Radioisotope Scanning,* Vol. 1, IAEA, 1964, p. 321.

18. Charleston, D. B., Beck, R. N., Fidelberg, P. and Schuh, M. W.: Techniques which aid in quantitative interpretation of scan data. In *Medical Radioisotope Scanning,* Vol. 1, IAEA, 1964, p. 321.

19. Brown, D. W.: Recent developments in digital computer analysis and display of the radioisotope scan. *J. Nucl. Med.* **6**:327, 1965.

20. Tauxe, W. N. and Chaapel, D. W.: Contrast enhancement of scanning procedure by high-speed computer. *J. Nucl. Med.* **6**:326, 1965.

21. Laughlin, J. S., Weber, D. A., Kenny, P. J. and Ritter, F.: Total body retention and localization scanning. *J. Nucl. Med.* **6**:327, 1965.

22. Weber, D. A., Kenny, P. J., Pochaczevsky, R., Corey, K. R. and Laughlin, J. S.: Liver scans with digital readout. *J. Nucl. Med.* **6**:528, 1965.

23. Harris, J. L.: Image evaluation and restoration. *J. Opt. Soc. Am.* **56**:569, 1966.

(Turn page for Appendix)